

## Chapter 5

# Spatial Distribution of Earthquake Potential along the Himalayan Arc

*“Training proves to be the key ingredient to handling any disaster.”*

by Walter Maddox

---

The present chapter focuses on the computation of the spatial distribution of earthquake potential by comparing the accumulated geodetic moment rates (calculated from strain rates) with the associated released seismic moment rates (calculated from  $\sim 900$  years of seismicity data) along different segments of the Himalayan arc.

---

### Contents

5.1	Introduction . . . . .	153
5.2	Study region and dataset . . . . .	154
5.3	Methodology . . . . .	155
5.3.1	Are the GPS-derived deformation signals comparable to the seismic signals? . . . . .	156
5.3.2	Seismogenic source segmentation for the present analysis . . . . .	157
5.3.3	Computation of seismic moment rate . . . . .	159
5.3.4	Computation of geodetic moment rate . . . . .	159
5.3.5	Computation of earthquake potential . . . . .	160
5.4	Results and discussion . . . . .	161
5.4.1	Moment rate ratio along the Himalayan arc . . . . .	161
5.4.2	Earthquake potential along the northwest Himalaya (Sec-1 to Sec-13) . . . . .	164

5.4.3	Earthquake potential along the central Himalaya (Sec-14 to Sec-22)	164
5.4.4	Earthquake potential along the northeast Himalaya (Sec-23 and Sec-24)	165
5.5	Sensitivity analysis	165
5.6	Summary	182

---

A part of this chapter has been published in the following refereed publication:

**Y. Sharma**, S. Pasari, K.E. Ching, O. Dikshit, T. Kato, J.N. Malik, C.P. Chang, and J.Y. Yen, “Spatial distribution of earthquake potential along the Himalayan arc”, *Tectonophysics*, vol. 791, pp. 228556, 2020. (SCI)  
(<https://doi.org/10.1016/j.tecto.2020.228556>)

## 5.1 Introduction

The region of highest seismic activity in south-central Asia is the Himalaya, where several large earthquakes in the past have resulted in tens of thousands of casualties. An  $M_w > 8$  earthquake has also been claimed to be overdue in the Himalayan orogen [30, 31, 93, 212, 211, 216, 276]. However, the estimated moment deficit, possible maximum magnitude and prospective location of future earthquakes certainly vary along the Himalayan arc [2, 27, 30, 34, 43, 212, 214, 215, 273, 277]. Therefore, with a high-resolution geodetic data and an updated earthquake catalog, re-evaluation of the spatial distribution of earthquake potential is essential to assess the contemporary seismic hazard along the Himalayan collision zone [235].

Two major components to assess the energy budget of a seismogenic area are the geodetic strain build-up rate and the stress release rate through earthquakes. Consequently, the comparison between the geodetic and seismic moment rates can be interpreted as a significant indicator of seismic hazard in a region [5, 170, 204, 235].

Ader et al. (2012) [2] estimated that the moment deficit rate along the locked Main Himalayan Thrust (MHT) is  $6.6 \pm 0.4 \times 10^{19}$  Nm/yr beneath the Nepal Himalaya. Similarly, Lindsey et al. (2018) [154] computed the total moment rate within Nepal over a 1000 km length of the MHT and observed that the estimated moment accumulation rate of  $4.8 \pm 0.3 \times 10^{19}$  Nm/yr is 27% lesser than the value estimated by Ader et al. (2012) [2]. Stevens and Avouac (2015) [277] found that the MHT is fully locked over a 100 km width and it builds up a moment deficit rate of about  $15.1 \pm 1 \times 10^{19}$  Nm/yr along the entire Himalayan arc. In addition, based on the analysis of earthquake catalog and geodetic data, Stevens and Avouac (2016) [276] proposed the possibility of a millenary  $M_w \sim 9.0$  earthquake in the Himalaya. Bungum et al. (2017) [43] also estimated the moment rate ( $\sim 4.3 \times 10^{19}$  Nm/yr), which is 70% lesser than that of Stevens and Avouac (2015) [277]. As a consequence, there have been several inconsistencies in the previous moment rate estimates. In fact, all of these above studies had aimed at large scale seismicity forecast along the India-Eurasia collision zone, which may lead to an overestimation of the earthquake potential, particularly in the rupture areas of previous large earthquakes, such as the 1803 Garhwal, 1905 Kangra, 1934 Nepal-Bihar, 2005 Kashmir and the 2015 Gorkha earthquake [2, 43, 277]. Moreover, keeping in mind that a series of large earthquakes have already occurred along the Himalayan arc in the last 200 years, does it still have high potential to experience a large-sized event in the near future? In this chapter, this

problem is addressed in terms of spatial distribution of earthquake potential along the Himalayan arc.

## 5.2 Study region and dataset

The current study region comprising the Himalayan arc extends from the Hindu Kush in the northwest to Bhutan in the northeast (Fig. 5.1). As mentioned before, the study region includes three megathrusts, namely the MCT, MBT, and the MFT, along with a décollement (MHT). This décollement serves as an interface between the downgoing Indian plate and the overriding Himalayas.

The geodetic observations reveal that the shallow portion of the MHT around the Lower and Sub-Himalaya is fully locked, where the interseismic strain is being accumulated [20, 154, 277, 316]. This accumulated strain may be released through major ( $M_w 7.0 - 7.9$ ) to great ( $M_w \geq 8.0$ ) earthquakes along the Himalayan arc [20, 154, 277, 316, 323]. Moreover, the rapid growth of urban population and infrastructure development along the Himalayan foothills and its adjacent IGP has increased the potential of catastrophic damage in future earthquakes. As a consequence, how to reasonably estimate the spatial distribution of Himalayan seismic hazard is an important issue, especially in the debated seismic gap (see Section 1.6 in Chapter 1).

To compute an updated and detailed segmentation-based earthquake potential along the Himalayan arc, two types of data are used, viz. GPS velocity data and 900 years of earthquake data. Recall that the surface velocity field comprising 486 horizontal signals along with the strain rate field have already been discussed in Chapter 3 (Fig. 3.23 and Fig. 3.25). Consequently, the earthquake data are acquired from global earthquake catalogs of the United States Geological Survey (USGS) and the International Seismological Centre (ISC), along with some published regional catalogs [e.g., 30, 129, 171, 202] spanning from 1100 to 2018. Earthquake magnitude before 1897 was estimated by spatial distribution of the intensities [30]. After scrutinizing duplicate entries, an integrated earthquake catalog containing a total of 11,553 events ( $M_w \geq 4.0$ ) since 1100 AD is obtained, including 11 events of  $M_w \geq 8.0$ . It may also be noted that the historical earthquake data before 1900 are obtained from Bilham (2019) [30] and Kayal (2008) [129], who have prepared an extensive catalog of Himalayan earthquakes. It is believed that Bilham (2019) [30] and Kayal (2008) [129] also have taken care of the uncertainties (if any) in size, location, or time for these Himalayan events, particularly for the

pre-instrumental events.

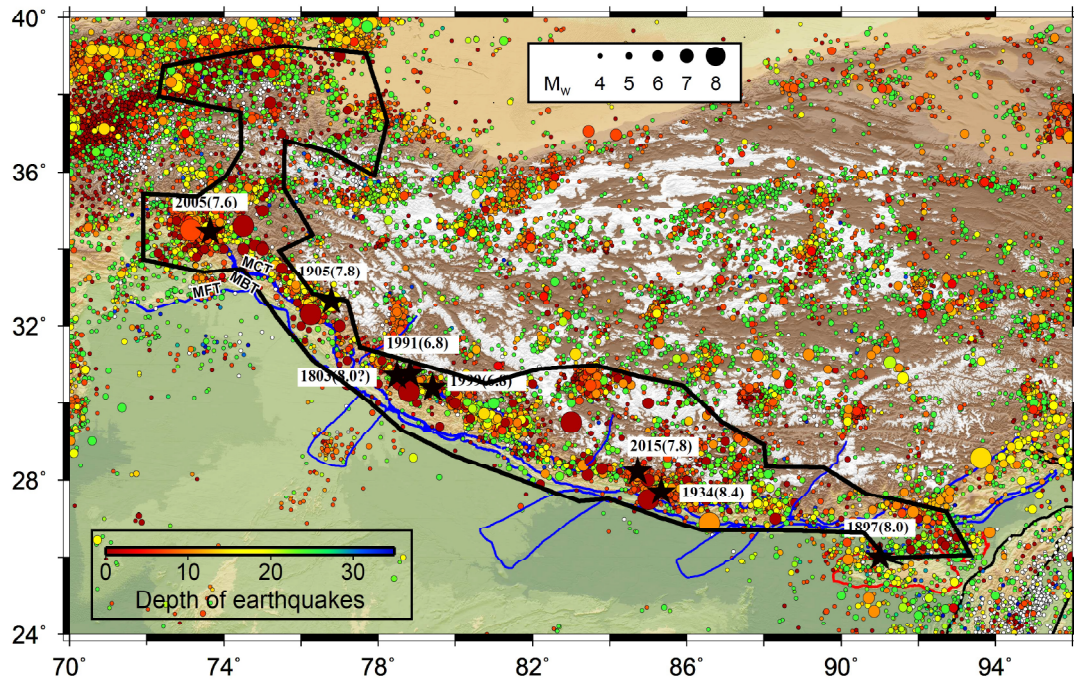


**Fig. 5.1:** Background seismicity along the study area (Himalaya); color and size of circles indicate depth and magnitude of earthquakes, respectively. The black polygon in the main figure represents the extent of the present study area.

### 5.3 Methodology

The derived strain rates (see Section 3.6) are translated into geodetic moment rates and compared with seismic moment rates calculated using 900 years of seismicity [9, 30, 49, 129, 202]. In the below subsections, the segmentation of the study area and computation of geodetic moment rate, seismic moment rate, and earthquake potential are addressed. In addition, some important issues regarding the comparability of geodetic signals to the seismic signals are also highlighted.

### 5.3.1 Are the GPS-derived deformation signals comparable to the seismic signals?

While the geodetic strain describes the crustal deformation in a region, the focal mechanism for an earthquake characterizes the dominant fault style of the source region, and there is not a single simple relation between the two [167]. To find the relationship between GPS deformation signals in the horizontal directions and seismic signals from observed seismicity, geodetic strain rates, and focal mechanism solutions of earthquakes since 1976 from Global Centroid Moment Tensor (GCMT) catalog are considered. In the present analysis, it is found that both (strain rates and focal mechanism) techniques exhibit similar tectonic deformation (extension or compression) pattern along the Himalayan arc (Fig. 5.2 and 5.3). For instance, in both Fig. 5.3 and Fig. 5.2,

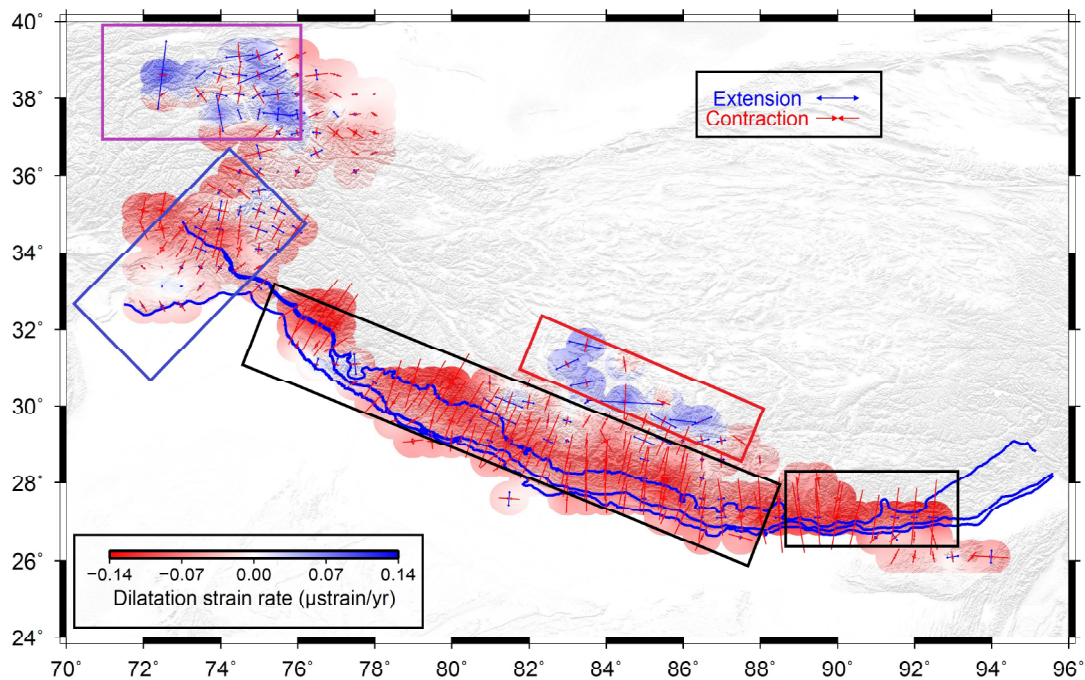


**Fig. 5.2:** Geodetic strain rates along the Himalayan arc (re-drawn from Fig. 3.25).

it is observed that (i) within the black rectangles ( $\sim 74^{\circ}\text{N}–88^{\circ}\text{N}$  to  $\sim 26^{\circ}\text{E}–33^{\circ}\text{E}$  and  $\sim 88^{\circ}\text{N}–93^{\circ}\text{N}$  to  $\sim 27^{\circ}\text{E}–28^{\circ}\text{E}$ ), a dominant compression mechanism (i.e., thrust faulting) is evident, (ii) within the blue rectangle ( $\sim 71^{\circ}\text{N}–77^{\circ}\text{N}$  to  $\sim 31^{\circ}\text{E}–37^{\circ}\text{E}$ ), a dominant thrust faulting along with minor normal faulting is present, (iii) the red rectangle ( $\sim 81^{\circ}\text{N}–88^{\circ}\text{N}$  to  $\sim 28^{\circ}\text{E}–33^{\circ}\text{E}$ ) encloses normal as well as oblique fault style, and (iv)

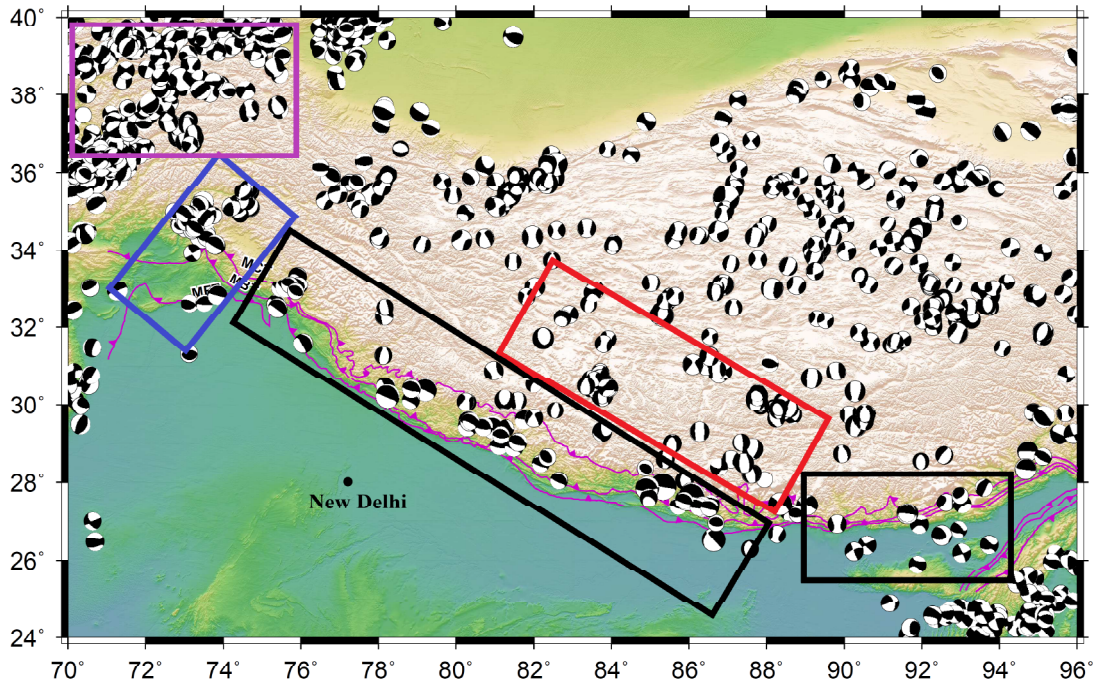


**Fig. 5.3:** Focal mechanism solution of Himalayan earthquakes since 1976.

the purple rectangle ( $\sim 71^\circ\text{N}$ – $76^\circ\text{N}$  to  $\sim 37^\circ\text{E}$ – $39^\circ\text{E}$ ) represents strike-slip and normal faulting. Therefore, from the above analysis, it seems reasonable to compare geodetic and seismic moment rates to determine the spatial distribution of earthquake potential along the Himalayan arc. The proposed methodology of comparison between geodetic and seismic moment rates is also guided by several such studies around the world [2, 43, 55, 105, 154, 204, 277, 303, 304].

### 5.3.2 Seismogenic source segmentation for the present analysis

In order to determine the spatial distribution of seismic hazard along the Himalayan arc, a segmentation-based approach is considered. To find some strong evidence for the criteria of segmentation, a summary of relevant studies is provided below.

1. Bilham et al. (2001) [34] divided the Himalayan arc into 10 regions, with lengths approximately corresponding to those of great Himalayan ruptures (220 km). However, they did not use any tectonic or subsurface topography for the division. A similar division has also been proposed by Bilham (2019) [30].

2. In Taiwan, Hsu et al. (2009) [104] have clearly mentioned that they examine those areas where there are at least 10 earthquakes and sufficient GPS data points.
3. In Greece, Chousianitis et al. (2015) [55] have also used a segmentation based approach and they examine only those areas which have sufficient GPS and earthquake data.

Guided by the above studies, the present analysis divides the study area into 24 seismogenic zones based on a two-fold criteria. First, the entire region is divided into three broader segments: northwest, central, and northeast Himalaya [2, 84]. Second, these three broader segments are further divided into 24 segments from the combination of the following points:

- (i) Each zone should contain at least 15 earthquakes of magnitude  $M_w \geq 4.0$ .
- (ii) Each zone should receive a sufficient amount of geodetic data points.
- (iii) Rupture area of any large earthquake should be bounded within a single segment.
- (iv) Almost all GPS data are being covered by these 24 segments.

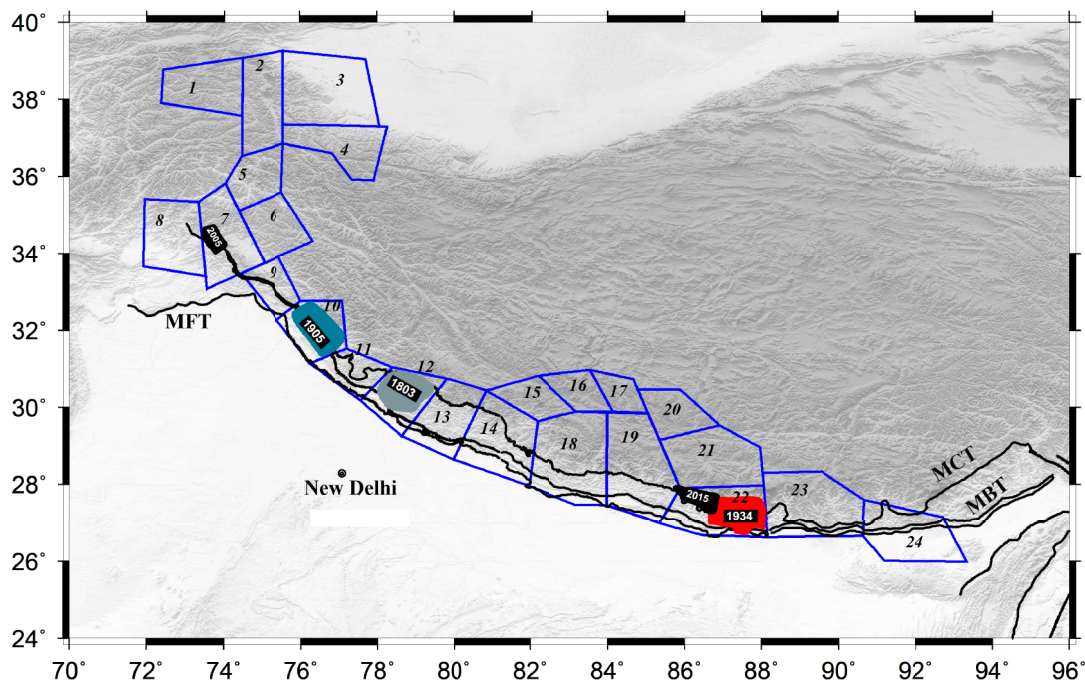


**Fig. 5.4:** Distribution of 24 segments of the Himalayan arc.

### 5.3.3 Computation of seismic moment rate

The seismic moment rates are estimated based on the earthquakes that have occurred since the 11<sup>th</sup> century. All magnitudes within the catalog are converted into moment magnitude in order to estimate the seismic moment corresponding to each event. The following relation is used for this purpose [127]:

$$M_0 = 10^{(1.5M_w+9.1)} \quad (5.1)$$

It has been observed that about 80% of total earthquakes in the considered catalog have a focal depth of 0–20 km. However, along the Himalayan arc, there are a few large earthquakes with focal depths 20–35 km. For example, according to Kayal (2008) [129], who have provided a revised earthquake catalog from 1505–2005 for India and its neighborhood, the 1905 Kangra, 1934 Nepal-Bihar, 1999 Chamoli, and the 2005 Kashmir earthquake have occurred at a depth of 25 km, 25 km, 21 km, and 26 km respectively. Similarly, Mukhopadhyay (2011) [184] examined earthquakes from 1905–2009 and suggested clustering of earthquakes parallel to MCT at a depth of 15–25 km and 35–45 km. Bilham (2019) [30] suggested that most of Himalayan earthquakes occur at shallow depths (<30 km). He also suggested that earthquakes with depths exceeding 40 km are relatively rare around the Himalayan region [30]. In addition, several geodetic studies [e.g., 2, 30, 154, 179, 219, 277] have suggested that Himalayan earthquakes occur along the décollement (MHT) at a depth of about 20 km. Therefore, guided by the above studies, the present analysis considers focal depth varying from 0–20 km, 0–25 km, 0–30 km, and 0–35 km for calculating seismic moment rate.

The estimated seismic moments are now converted into moment rates  $\dot{M}_0^s$  by dividing the length of the catalog for every segment. To balance the moment on each seismic zone, a catalog length spanning one or more seismic cycles is considered. Based on the available literature [e.g., 31, 40, 95, 117, 146, 161, 164, 180, 190, 219, 227, 228, 277, 306, 308], it is believed that the present catalog spanning about 900 years of data corresponds to one seismic cycle of great Himalayan earthquakes.

### 5.3.4 Computation of geodetic moment rate

The estimated strain rates are presumed to be as the basis for calculating geodetic moment rates. The strain rate tensors are utilized to derive scalar geodetic moment rate using the

equation given by Savage and Simpson (1997) [252].

$$\dot{M}_0^g = 2\mu H_c A_c \text{Max}(|\dot{\epsilon}_1|, |\dot{\epsilon}_2|, |\dot{\epsilon}_1 + \dot{\epsilon}_2|) \quad (5.2)$$

Here,  $\dot{M}_0^g$  is the geodetic moment rate;  $\mu=3 \times 10^{10} \text{ N/m}^2$  is the shear modulus of the elastic layer;  $H_c$  is the seismogenic thickness, which also varies from 20 km to 35 km as mentioned in the above section;  $A_c$  is the area of the source zone; and  $\dot{\epsilon}_1$  and  $\dot{\epsilon}_2$  are the maximum and minimum principal strain rates, respectively. The moment rate estimated from the geodetic strain rate is proportional to the chosen seismogenic thickness.

### 5.3.5 Computation of earthquake potential

To calculate the current earthquake potential in a segment, the moment deficit rate is calculated by subtracting the seismic moment rate from the geodetic moment rate as

$$\dot{M}_0^g - \dot{M}_0^s = \dot{M}_0 \quad (5.3)$$

To derive the required amount of earthquake magnitude, the moment rate ratio is calculated as

$$\text{Moment rate ratio} = \dot{M}_0^g - \dot{M}_0^s = K \text{ (assuming)} \quad (5.4)$$

Three cases evolve:

1. If  $K > 1$ , then the geodetic moment rate (energy accumulation) would be higher than the seismic moment rate (energy release). Considering the hypothesis that the total moment deficit rate can be expressed in terms of future earthquakes, the amount of required seismic activity is determined to completely remove the discrepancy between the geodetic and seismic moment rate (that is to make the moment rate ratio unity) [55, 90, 204].
2. If  $K=1$ , then this implies that the geodetic moment rate is equal to the seismic moment rate. This means that the accumulated energy is leveled by the background seismicity.
3. If  $K < 1$ , then seismic moment rate is higher than the geodetic moment rate. This implies that the accumulated strain energy is completely released and the corresponding region is accumulating seismic energy in the interseismic period.

## 5.4 Results and discussion

The budget of earthquake potential along the Himalayan arc is calculated by comparing the geodetic and seismic moment rates. The geodetic observations include the contribution of seismic strain accumulation and aseismic strain release, while the seismic data show the seismic strain release [55]. As a result, the comparison of geodetic and seismic moment rates provides valuable information about the deformation mechanism and earthquake moment production [55].

### 5.4.1 Moment rate ratio along the Himalayan arc

An overview of the comparison is achieved in terms of the ratio of geodetic to the seismic moment rates (Table 5.1 and Fig. 5.5). A good agreement on this comparison with a moment ratio close to unity is observed in two zones of each Kashmir Himalaya (Sec-6 and Sec-7) and southern Tibet (Sec-15 and Sec-16) as well as one zone of each Himachal region (Sec-10) and eastern Nepal (Sec-19). Another significant level of agreement with a ratio of about two has been observed in Sec-9, Sec-18, and Sec-23. However, in Sec-12 and Sec-22, a high seismic moment release rate is observed in comparison to the moment accumulation rate, resulting in a moment ratio below unity. In contrast, in segments Sec-4, Sec-5, Sec-8, Sec-11, Sec-21, and Sec-24, the geodetic moment rates are enormously higher than the seismic ones (moment ratio  $\geq 50$ ), probably due to the under-sampling of the long-term earthquake rates, long-term aseismic crustal deformation, or a composite of these two factors [55]. In other source zones, the geodetic moment rates are moderately higher by a factor of 3 to 20 (Table 5.1). From the above results, it may be noted that a higher moment rate ratio does not necessarily imply a higher earthquake potential.

Considering the hypothesis that the complete moment deficit rate in a segment will be released by one or more earthquakes within the segment, the maximum size of possible earthquake is determined to eliminate the mismatch between the geodetic and the seismic moment rates [43, 55, 204]. The results are summarized in Table 5.1 and Fig. 5.5.

**Table 5.1:** Summary of comparison between geodetic moment rate and seismic moment rate calculated at 25 km seismogenic depth for different segments (using  $\geq 900$ ); dash (-) in the earthquake potential column denotes no seismic potential.

Area	$\dot{M}_0^g$ ( $10^{17}$ Nm/yr)	$\dot{M}_0^s$ ( $10^{17}$ Nm/yr)	$\dot{M}_0^g/\dot{M}_0^s$	Current earthquake potential ( $M_w$ )
1	58.91±5.60	19.12	3.1	7.6
2	46.50±2.06	6.57	7.1	7.7
3	83.50±7.81	3.84	21.7	7.7
4	38.20±2.09	0.59	65.1	7.4
5	25.30±2.24	0.37	68.6	7.5
6	28.50±2.37	27.35	1.1	6.5
7	80.50±4.46	75.20	1.1	5.7
8	66.40±3.14	1.14	58.4	7.7
9	26.90±1.25	10.30	2.6	7.5
10	54.90±2.89	50.90	1.1	6.5
11	32.90±1.16	0.62	53.1	7.7
12	51.80±3.52	88.39	0.6	-
13	63.50±2.19	8.70	7.3	8.0
14	76.90±3.12	6.10	12.6	8.0
15	22.60±1.17	20.67	1.1	7.3
16	23.90±1.76	18.8	1.3	6.6
17	16.70±1.39	2.82	5.9	7.2
18	93.00±8.14	51.20	1.8	8.1
19	102.20±8.57	90.78	1.1	8.0
20	23.60±1.32	1.50	15.7	7.5
21	70.80±6.54	0.99	71.5	7.7

22	$61.10 \pm 4.10$	513.00	0.1	–
23	$92.30 \pm 7.18$	43.88	2.1	8.2
24	$80.40 \pm 7.41$	1.48	54.3	8.2

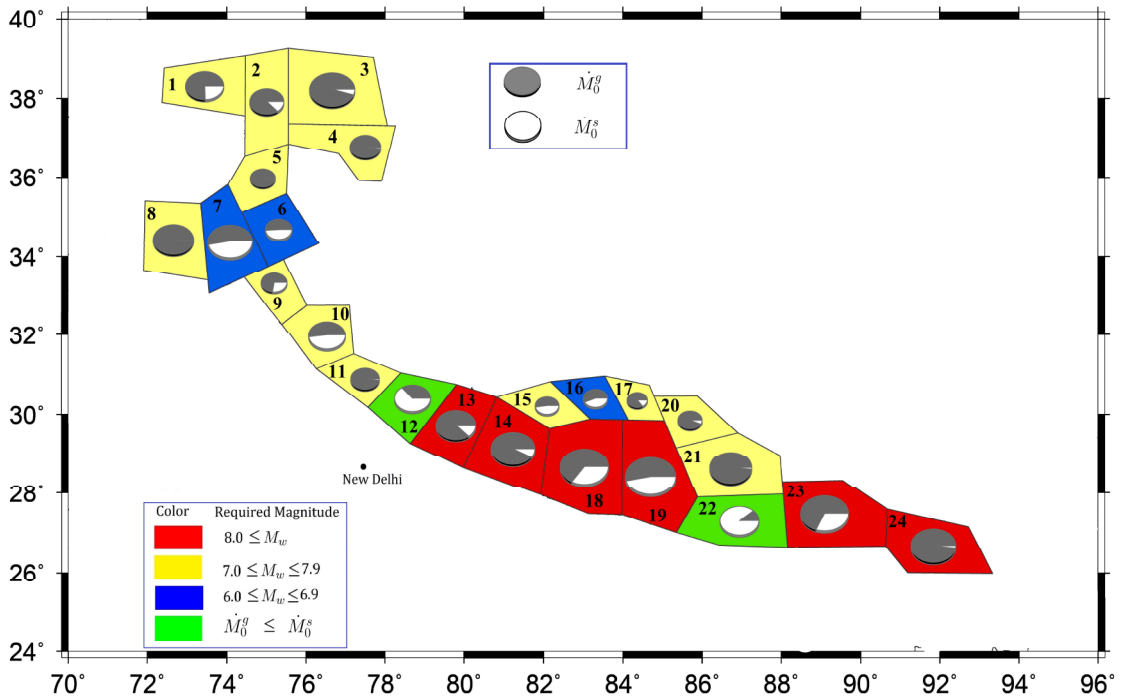


**Fig. 5.5:** Distribution of earthquake potential and moment rate ratio along the Himalayan arc. While the color of a segment indicates the current seismic potential in terms of the maximum magnitude, the pie chart in a segment graphically represents the derived moment rate ratio. The size of a circle indicates the accumulated geodetic moment rate in a segment, whereas the fraction of it that has been released is shown by the white slice of the circle. A pie chart filled with half gray and half white illustrates the unit moment rate ratio.

The regions where no large Himalayan earthquakes have occurred in the last 100 years are found to be most likely to experience one in the study region. To illustrate further, the results of earthquake potential along three broader segments of the Himalayan arc, namely the northwest Himalaya, central Himalaya, and the northeast Himalaya are discussed below.

### 5.4.2 Earthquake potential along the northwest Himalaya (Sec-1 to Sec-13)

The northwest Himalaya comprises first thirteen sections of the total 24 segments. The maximum possible magnitude of prospective earthquakes along these segments varies from  $M_w=5.7$  to  $M_w=8.0$  (Table 5.1). More specifically, the current earthquake potential in each of Sec-1 to Sec-5 is observed to be  $M_w \geq 7.5$ ; Sec-6 has a potential of a strong earthquake ( $M_w \geq 6.5$ ); Sec-7, that covers the rupture area of the 2005 Kashmir earthquake, currently has the possibility of a moderate sized earthquake ( $M_w \geq 5.7$ ). The recurrence interval of the 2005 Kashmir event turns out to be  $615 \pm 100$  years, which agrees to the return period ( $680 \pm 150$  years) estimated by Bendick et al. (2006) [24]. In each of Sec-8 and Sec-9, there is a possibility of a major earthquake ( $M_w \geq 7.5$ ) in the near future; Sec-10, which experienced the 1905 Kangra earthquake, currently holds energy equivalent to a strong event; Sec-11, with a high moment rate ratio of 53, has the current potential of a major earthquake ( $M_w \geq 7.7$ ); Sec-12, enclosing the rupture zones of the 1803 Garhwal earthquake, 1991 Uttarkashi earthquake, and the 1999 Chamoli earthquake, shows a balanced moment deficit rate (Table 5.1). However, the neighboring segment, Sec-13, has sufficient amount of moment deficit rate ( $5.8 \times 10^{18}$  Nm/yr) to produce a great ( $M_w \geq 8.0$ ) earthquake. This moment deficit rate is about 30% lesser than the estimated moment deficit rate ( $8.4 \pm 1 \times 10^{18}$  Nm/yr) of Ponraj et al. (2019) [219].

### 5.4.3 Earthquake potential along the central Himalaya (Sec-14 to Sec-22)

The central part of the Himalaya (i.e., Nepal and Tibet) comprises nine segments, Sec-14 to Sec-22. In Sec-14, Sec-18, and Sec-19, the mismatch between the geodetic and seismic moment rates provides the potential of a great earthquake ( $M_w \geq 8.0$ ) in each zone. Furthermore, as these sections belong to the debated central seismic gap [30, 34, 43, 273], the potential of a great earthquake in these segments is reasonable. The geodetic moment rate of  $1.20 \times 10^{19}$  Nm/yr in these segments is very high in comparison to other segments of the Himalayan arc. In contrast, the nearby segment (Sec-22) in the eastern Nepal shows that the stored energy over the past 900 years has been balanced by observed seismicity. This is due to the fact that the accumulated strain energy has been released in the 1934 Nepal-Bihar earthquake and the 2015 Gorkha earthquake. However, the possibility of a great event remains high in the west of Sec-22 (i.e., Sec-19). The results

in the Nepal Himalaya is consistent to the findings of Sreejith et al. (2018) [272] and Wyss and Chamlagain (2019) [313], who have suggested that the 2015 Nepal earthquake along with its aftershocks has partially removed the accumulated strain along the MHT. They have also suggested a possible location of future large earthquake in the west (Sec-14, Sec-18, and Sec-19) or in the south of the epicenter of 2015 Gorkha earthquake [272, 313]. The remaining segments, Sec-15 to Sec-17, Sec-20, and Sec-21, belong to the southern Tibet in the north of Nepal Himalaya. In these segments, low moment deficit rates of  $1.93 \times 10^{17}$  Nm/yr to  $6.98 \times 10^{18}$  Nm/yr indicate current earthquake potential of  $M_w \geq 7.3$ ,  $M_w \geq 6.6$ ,  $M_w \geq 7.2$ ,  $M_w \geq 7.5$ , and  $M_w \geq 7.7$ , respectively (Table 5.1).

#### 5.4.4 Earthquake potential along the northeast Himalaya (Sec-23 and Sec-24)

The last two regions (Sec-23 and Sec-24) of the present segmentation belong to the northeast part of the Himalaya (Bhutan Himalaya) (Table 5.1). These sections have stored 72% moment deficit rate at present time with the capability to generate a great earthquake of magnitude  $M_w \geq 8.2$  in each segment. The above estimation is corroborated by the previous findings of Bilham et al. (2001) [34], Barman et al. (2016) [22], and Bilham (2019) [30] as well as the quiescence of historical great earthquakes in these segments.

### 5.5 Sensitivity analysis

To account for the sensitivity in the final earthquake potential for a given segment, first, the earthquake focal depth (20 km to 35 km) is varied individually and its effects on the computed earthquake potential are noted (Table 5.2 to Table 5.5). Second, different catalog spans (keeping the earthquake depth, say 25 km, fixed) such as  $\leq 200$  years,  $\sim 500$  years, and  $\geq 900$  years are used and their effects on the computed earthquake potential are noted. Third, to account for the uncertainty in the estimated geodetic moment rates (for a fixed earthquake depth, say 25 km), the lower limit  $((\dot{M}_0^g)_{min})$  and upper limit  $((\dot{M}_0^g)_{max})$ , are chosen, and its impact on the final earthquake potential for a segment is observed (Table 5.10 to Table 5.12). Finally, the contribution of aseismic deformation on the earthquake potential is computed by reducing 1/3 of the total geodetic strain accumulation due to the aseismic activities as suggested by Stevens and Avouac (2015) [277] (Table 5.13

and Table 5.14). It may be noted that the impact of the choice of the smoothing parameter in total strain rate has already been discussed in Section 3.5 of Chapter 3. The below tables summarize the amount of uncertainty in the resultant earthquake potential for each parameter (mentioned above) in each segment.

**Table 5.2:** Geodetic and seismic moment rates, moment rate ratio, moment deficit, and earthquake potential using the seismogenic depth as 20 km; dash (–) in the earthquake potential column denotes no seismic potential.

Area	$\dot{M}_0^g$ ( $10^{17}$ Nm/yr)	$\dot{M}_0^s$ ( $10^{17}$ Nm/yr)	$\dot{M}_0^g/\dot{M}_0^s$	$\dot{M}_0$ ( $10^{20}$ Nm)	Earthquake potential ( $M_w$ )
1	47.13±4.48	19.02	2.5	3.008	7.6
2	37.20 ±1.65	6.56	5.7	3.769	7.7
3	66.80±6.25	3.84	17.4	4.407	7.6
4	30.56±1.67	0.48	63.7	1.594	7.4
5	20.24±1.79	0.36	56.2	1.789	7.4
6	22.80±1.89	27.30	0.8	–0.315	–
7	64.40±3.57	75.10	0.9	–0.519	–
8	53.12±2.51	1.08	49.2	4.684	7.7
9	21.52±1.00	10.26	2.1	1.689	7.4
10	43.92±2.31	49.10	0.9	–0.518	–
11	26.32±0.93	0.57	46.2	4.120	7.7
12	41.44±2.82	86.52	0.5	–9.692	–
13	50.80±1.75	8.70	5.8	12.420	8.0
14	61.52±2.49	6.10	10.1	11.084	8.0
15	18.08±0.94	17.80	1	0.171	6.8
16	19.12±1.41	13.67	1.3	0.114	6.6
17	13.36±1.11	2.81	4.8	0.686	7.2
18	74.40±6.51	51.20	1.5	11.832	8.0

19	81.76±6.86	90.71	0.9	-8.216	-
20	18.88±1.06	1.48	12.8	1.949	7.5
21	56.64±5.23	0.79	71.7	4.468	7.7
22	48.88±3.21	512.00	0.1	-50.943	-
23	73.84±5.74	43.20	1.7	15.320	8.1
24	64.32±5.93	1.48	43.5	18.098	8.1

**Table 5.3:** Geodetic and seismic moment rates, moment rate ratio, moment deficit, and earthquake potential using the seismogenic depth as 30 km; dash (-) in the earthquake potential column denotes no seismic potential.

Area	$\dot{M}_0^g$ ( $10^{17}$ Nm/yr)	$\dot{M}_0^s$ ( $10^{17}$ Nm/yr)	$\dot{M}_0^g/\dot{M}_0^s$	$\dot{M}_0$ ( $10^{20}$ Nm)	Earthquake Potential ( $M_w$ )
1	70.69±6.72	19.27	3.7	5.502	7.8
2	55.80±2.47	6.58	8.5	6.054	7.8
3	100.2±9.37	3.84	26.1	6.745	7.8
4	45.84±2.51	0.63	72.8	2.396	7.5
5	30.36±2.69	0.39	77.8	2.697	7.6
6	34.20±2.84	27.40	1.3	0.476	7.1
7	96.60±5.35	75.24	1.3	1.047	7.3
8	79.68±3.77	1.51	52.8	7.035	7.8
9	32.28±1.50	10.32	3.1	3.294	7.6
10	65.88±3.47	50.91	1.3	1.497	7.4
11	39.48±1.39	0.63	62.7	6.216	7.8
12	62.16±4.22	88.39	0.7	-5.637	-
13	76.20±2.63	8.71	8.7	19.910	8.1
14	92.28±3.74	6.15	15	17.226	8.1

15	27.12±1.41	20.70	1.3	3.916	7.7
16	28.68±2.11	19.10	1.5	0.201	6.8
17	20.04±1.67	2.83	7.1	1.119	7.3
18	111.60±9.77	51.24	2.2	30.784	8.3
19	122.64±10.28	90.78	1.4	29.247	8.2
20	28.32±1.58	1.51	18.8	3.003	7.6
21	84.96±7.84	0.99	85.8	6.718	7.8
22	73.32±4.81	513.00	0.2	-48.365	-
23	110.76±8.62	43.90	2.5	33.430	8.3
24	96.48±8.89	1.50	64.3	27.354	8.2

**Table 5.4:** Geodetic and seismic moment rates, moment rate ratio, moment deficit, and earthquake potential using the seismogenic depth as 35 km; dash (-) in the earthquake potential column denotes no seismic potential.

Area	$\dot{M}_0^g$ ( $10^{17}$ Nm/yr)	$\dot{M}_0^s$ ( $10^{17}$ Nm/yr)	$\dot{M}_0^g/\dot{M}_0^s$	$\dot{M}_0$ ( $10^{20}$ Nm)	Earthquake Potential ( $M_w$ )
1	82.48±7.84	20.10	4.1	6.674	7.8
2	65.10±2.89	6.71	9.7	7.182	7.8
3	116.90±10.94	3.91	29.9	7.910	7.9
4	53.48±2.92	0.67	79.8	2.799	7.6
5	35.42±3.13	1.34	26.4	3.067	7.6
6	39.90±3.31	33.16	1.2	0.612	7.1
7	112.70±6.25	78.65	1.4	1.668	7.3
8	92.96±4.39	2.23	41.7	8.166	7.9
9	37.66±1.75	10.82	3.5	4.026	7.7
10	76.86±4.04	55.90	1.4	2.096	7.5

11	46.06±1.63	0.80	57.6	7.242	7.8
12	72.52±4.94	89.33	0.8	-3.614	-
13	88.90±3.06	8.76	10.1	23.641	8.2
14	107.66±4.36	7.56	14.2	20.020	8.1
15	31.64±1.65	20.94	1.5	6.527	7.8
16	33.46±2.47	21.17	1.6	0.258	6.9
17	23.38±1.94	2.99	7.8	1.325	7.3
18	130.20±11.39	51.31	2.5	40.234	8.3
19	143.08±12.01	91.52	1.6	47.332	8.3
20	33.04±1.86	1.51	21.9	3.531	7.6
21	99.12±9.15	1.11	89.3	7.841	7.9
22	85.54±5.62	513.00	0.2	-47.021	-
23	129.22±10.05	45.10	2.9	42.060	8.3
24	112.56±10.38	2.04	55.2	31.830	8.3

**Table 5.5:** Summarization of earthquake potential at varying seismological depth (20 km to 35 km); dash (-) in the earthquake potential columns denote no seismic potential.

Area	Earthquake potential ( $M_w$ ) at 20 km depth	Earthquake potential ( $M_w$ ) at 25 km depth	Earthquake potential ( $M_w$ ) at 30 km depth	Earthquake potential ( $M_w$ ) at 35 km depth	Earthquake potential range ( $M_w$ )
1	7.6	7.7	7.8	7.8	7.6–7.8
2	7.7	7.7	7.8	7.8	7.7–7.8
3	7.7	7.8	7.8	7.9	7.7–7.9
4	7.4	7.5	7.5	7.6	7.4–7.6
5	7.4	7.5	7.6	7.6	7.4–7.6
6	-	6.5	7.1	7.1	6.5–7.1

7	–	5.7	7.2	7.3	5.7–7.3
8	7.7	7.8	7.8	7.9	7.7–7.9
9	7.4	7.5	7.6	7.7	7.4–7.7
10	–	6.6	7.4	7.5	6.6–7.5
11	7.7	7.7	7.8	7.8	7.7–7.8
12	–	–	–	–	–
13	8.0	8.1	8.1	8.2	8.0–8.2
14	8.0	8.0	8.1	8.1	8.0–8.1
15	6.8	7.3	7.7	7.8	6.8–7.8
16	6.6	6.6	6.8	6.9	6.6–6.9
17	7.2	7.2	7.3	7.3	7.2–7.3
18	8.0	8.2	8.3	8.3	8.0–8.3
19	–	8.1	8.2	8.3	8.1–8.3
20	7.5	7.5	7.6	7.6	7.5–7.6
21	7.7	7.8	7.8	7.9	7.7–7.9
22	–	–	–	–	–
23	8.1	8.2	8.3	8.3	8.1–8.3
24	8.1	8.2	8.2	8.3	8.1–8.3

**Table 5.6:** Geodetic and seismic moment rates, moment rate ratio, moment deficit, and earthquake potential using  $\leq 200$  years of earthquake catalog span (at a fixed depth 25 km); dash (–) in the earthquake potential column denotes no seismic potential.

Area	$\dot{M}_0^g$ ( $10^{17}$ Nm/yr)	$\dot{M}_0^s$ ( $10^{17}$ Nm/yr)	$\dot{M}_0^g/\dot{M}_0^s$	$\dot{M}_0$ ( $10^{20}$ Nm)	Earthquake Potential ( $M_w$ )
1	58.91 $\pm$ 5.60	19.12	3.1	4.258	7.6
2	46.50 $\pm$ 2.06	6.57	7.1	4.911	7.7

3	83.50±7.81	3.84	21.7	5.576	7.7
4	38.20±2.09	0.59	65.1	1.993	7.4
5	25.30±2.24	0.37	68.6	2.244	7.5
6	28.50±2.37	1.01	28.2	3.39	7.6
7	80.50±4.46	35.87	2.2	8.53	7.8
8	66.40±3.14	2.04	32.55	10.68	7.9
9	26.90±1.25	10.30	2.6	2.490	7.5
10	54.90±2.89	50.90	1.1	0.100	6.5
11	32.90±1.16	0.17	193.5	5.238	7.7
12	51.80±3.52	6.52	7.94	7.969	7.8
13	63.50±2.19	1.51	42.1	11.345	8.0
14	76.90±3.12	6.10	12.6	14.160	8.0
15	22.60±1.17	20.67	1.1	1.177	7.3
16	23.90±1.76	18.8	1.3	0.107	6.6
17	16.70±1.39	2.82	5.9	0.902	7.2
18	93.00±8.14	13.78	6.7	6.021	7.8
19	102.20±8.57	61.24	1.7	12.633	8.0
20	23.60±1.32	1.50	15.7	2.475	7.5
21	70.80±6.54	0.99	71.5	5.585	7.7
22	61.10±4.10	513.00	0.1	-49.709	-
23	92.30±7.18	43.88	2.1	24.210	8.2
24	80.40±7.41	3.01	27.0	13.466	8.0

**Table 5.7:** Geodetic and seismic moment rates, moment rate ratio, moment deficit, and earthquake potential using  $\sim 500$  years of earthquake catalog span (at a fixed depth 25 km); dash (–) in the earthquake potential column denotes no seismic potential.

Area	$\dot{M}_0^g$ ( $10^{17}$ Nm/yr)	$\dot{M}_0^s$ ( $10^{17}$ Nm/yr)	$\dot{M}_0^g/\dot{M}_0^s$	$\dot{M}_0$ ( $10^{20}$ Nm)	Earthquake Potential ( $M_w$ )
1	58.91±5.60	19.12	3.1	4.258	7.6
2	46.50±2.06	6.57	7.1	4.911	7.7
3	83.50±7.81	3.84	21.7	5.576	7.7
4	38.20±2.09	0.59	65.1	1.993	7.4
5	25.30±2.24	0.37	68.6	2.244	7.5
6	28.50±2.37	27.35	1.1	0.081	6.5
7	80.50±4.46	75.20	1.1	0.005	5.7
8	66.40±3.14	1.14	58.4	5.873	7.7
9	26.90±1.25	10.30	2.6	2.490	7.5
10	54.90±2.89	50.90	1.1	0.100	6.5
11	32.90±1.16	0.17	193.5	5.238	7.7
12	51.80±3.52	88.39	0.6	–7.867	–
13	63.50±2.19	8.70	7.3	16.166	8.0
14	76.90±3.12	6.10	12.6	14.160	8.0
15	22.60±1.17	20.67	1.1	1.177	7.3
16	23.90±1.76	18.8	1.3	0.107	6.6
17	16.70±1.39	2.82	5.9	0.902	7.2
18	93.00±8.14	13.78	6.7	6.021	7.8
19	102.20±8.57	61.24	1.7	12.633	8.0
20	23.60±1.32	1.50	15.7	2.475	7.5
21	70.80±6.54	0.99	71.5	5.585	7.7

22	61.10±4.10	513.00	0.1	-49.709	-
23	92.30±7.18	43.88	2.1	24.210	8.2
24	80.40±7.41	1.48	54.3	22.729	8.2

**Table 5.8:** Geodetic and seismic moment rates, moment rate ratio, moment deficit, and earthquake potential using  $\geq 900$  years of earthquake catalog span (at a fixed depth 25 km); dash (-) in the earthquake potential column denotes no seismic potential.

Area	$\dot{M}_0^g$ ( $10^{17}$ Nm/yr)	$\dot{M}_0^s$ ( $10^{17}$ Nm/yr)	$\dot{M}_0^g/\dot{M}_0^s$	$\dot{M}_0$ ( $10^{20}$ Nm)	Earthquake Potential ( $M_w$ )
1	58.91±5.60	19.12	3.1	4.258	7.6
2	46.50±2.06	6.57	7.1	4.911	7.7
3	83.50±7.81	3.84	21.7	5.576	7.7
4	38.20±2.09	0.59	65.1	1.993	7.4
5	25.30±2.24	0.37	68.6	2.244	7.5
6	28.50±2.37	27.35	1.1	0.081	6.5
7	80.50±4.46	75.20	1.1	0.005	5.7
8	66.40±3.14	1.14	58.4	5.873	7.7
9	26.90±1.25	10.30	2.6	2.490	7.5
10	54.90±2.89	50.90	1.1	0.100	6.5
11	32.90±1.16	0.62	53.1	5.165	7.7
12	51.80±3.52	88.39	0.6	-7.867	-
13	63.50±2.19	8.70	7.3	16.166	8.0
14	76.90±3.12	6.10	12.6	14.160	8.0
15	22.60±1.17	20.67	1.1	1.177	7.3
16	23.90±1.76	18.8	1.3	0.107	6.6
17	16.70±1.39	2.82	5.9	0.902	7.2

18	93.00±8.14	51.20	1.8	21.318	8.1
19	102.20±8.57	90.78	1.1	15.074	8.0
20	23.60±1.32	1.50	15.7	2.475	7.5
21	70.80±6.54	0.99	71.5	5.585	7.7
22	61.10±4.10	513.00	0.1	-49.709	-
23	92.30±7.18	43.88	2.1	24.210	8.2
24	80.40±7.41	1.48	54.3	22.729	8.2

**Table 5.9:** Summarization of earthquake potential variation at different catalog span from  $\leq 200$  years to  $\geq 900$  years (at a fixed depth 25 km); dash (-) in the earthquake potential columns denote no seismic potential.

Area	Earthquake potential ( $M_w$ ) at $\leq 200$ years	Earthquake potential ( $M_w$ ) at $\sim 500$ years	Earthquake potential ( $M_w$ ) at $\geq 900$ years	Earthquake potential range ( $M_w$ )
1	7.6	7.6	7.6	7.6
2	7.7	7.7	7.7	7.7
3	7.7	7.7	7.7	7.7
4	7.4	7.4	7.4	7.4
5	7.5	7.5	7.5	7.5
6	7.6	6.5	6.5	6.5–7.6
7	7.8	5.7	5.7	5.7–7.8
8	7.9	7.7	7.7	7.7–7.9
9	7.5	7.5	7.5	7.5
10	6.5	6.5	6.5	6.5
11	7.7	7.7	7.7	7.7
12	7.8	-	-	7.8

13	8.0	8.0	8.0	8.0
14	8.0	8.0	8.0	8.0
15	7.3	7.3	7.3	7.3
16	6.6	6.6	6.6	6.6
17	7.2	7.2	7.2	7.2
18	7.8	7.8	8.1	7.8–8.1
19	8.0	8.0	8.0	8.0
20	7.5	7.5	7.5	7.5
21	7.7	7.7	7.7	7.7
22	–	–	–	–
23	8.2	8.2	8.2	8.2
24	8.0	8.2	8.2	8.0–8.2

**Table 5.10:** Geodetic and seismic moment rates, moment rate ratio, moment deficit, and earthquake potential using the minimum of geodetic moment rate (at a fixed depth 25 km); dash (–) in the earthquake potential column denotes no seismic potential.

Area	$\dot{M}_0^g$ ( $10^{17}$ Nm/yr)	$(\dot{M}_0^g)_{min}$ ( $10^{17}$ Nm/yr)	$\dot{M}_0^s$ ( $10^{17}$ Nm/yr)	$(\dot{M}_0^g)_{min}/\dot{M}_0^s$	$\dot{M}_0$ ( $10^{20}$ Nm)	Earthquake potential ( $M_w$ )
1	58.91±5.60	53.31	19.12	2.8	3.658	7.5
2	46.50±2.06	44.44	6.57	6.8	4.658	7.6
3	83.50±7.81	75.69	3.84	19.7	5.030	7.6
4	38.20±2.09	36.11	0.59	61.2	1.883	7.3
5	25.30±2.24	23.06	0.37	62.3	2.042	7.4
6	28.50±2.37	26.13	27.35	1.0	–0.085	–
7	80.50±4.46	76.04	75.20	0.9	–0.214	–

8	66.40±3.14	63.26	1.14	55.5	5.591	7.6
9	26.90±1.25	25.65	10.30	2.5	2.303	7.4
10	54.90±2.89	52.01	50.90	1.0	-0.189	-
11	32.90±1.16	31.74	0.62	51.2	4.979	7.6
12	51.80±3.52	48.28	88.39	0.5	-8.624	-
13	63.50±2.19	61.31	8.70	7.0	15.520	8.0
14	76.90±3.12	73.78	6.10	12.1	13.536	8.0
15	22.60±1.17	21.43	20.67	1.0	0.464	7.0
16	23.90±1.76	22.14	18.80	1.2	0.070	6.5
17	16.70±1.39	15.31	2.82	5.4	0.812	7.1
18	93.00±8.14	84.86	51.20	1.7	17.167	8.0
19	102.20±8.57	93.63	90.78	1.1	7.206	7.8
20	23.60±1.32	22.28	1.50	14.9	2.327	7.5
21	70.80±6.54	64.26	0.99	64.9	5.062	7.7
22	61.10±4.10	57.00	513.00	0.1	-50.160	-
23	92.30±7.18	85.12	43.88	1.9	20.620	8.1
24	80.40±7.41	72.99	1.48	49.3	20.595	8.1

**Table 5.11:** Geodetic and seismic moment rates, moment rate ratio, moment deficit, and earthquake potential using the maximum of geodetic moment rate (at a fixed depth 25 km); dash (-) in the earthquake potential column denotes no seismic potential.

Area	$\dot{M}_0^g$ ( $10^{17}$ Nm/yr)	$(\dot{M}_0^g)_{max}$ ( $10^{17}$ Nm/yr)	$\dot{M}_0^s$ ( $10^{17}$ Nm/yr)	$(\dot{M}_0^g)_{max}/\dot{M}_0^s$	$\dot{M}_0$ ( $10^{20}$ Nm)	Earthquake potential ( $M_w$ )
1	58.91±5.60	64.51	19.12	3.4	4.857	7.7
2	46.50±2.06	48.56	6.57	7.4	5.165	7.7

3	83.50±7.81	91.31	3.84	23.8	6.123	7.8
4	38.20±2.09	40.29	0.59	68.3	2.104	7.5
5	25.30±2.24	27.54	0.37	74.4	2.445	7.5
6	28.50±2.37	30.87	27.35	1.1	0.246	6.9
7	80.50±4.46	84.96	75.20	1.1	0.223	6.8
8	66.40±3.14	69.54	1.14	61.0	6.156	7.8
9	26.90±1.25	28.15	10.30	2.7	2.678	7.6
10	54.90±2.89	57.79	50.90	1.1	0.389	7.0
11	32.90±1.16	34.06	0.62	54.9	5.350	7.8
12	51.80±3.52	55.32	88.39	0.6	-7.110	–
13	63.50±2.19	65.69	8.70	7.6	16.812	8.1
14	76.90±3.12	80.02	6.10	13.1	14.784	8.0
15	22.60±1.17	23.77	20.67	1.1	1.891	7.5
16	23.90±1.76	25.66	18.80	1.4	0.144	6.7
17	16.70±1.39	18.09	2.82	6.4	0.993	7.3
18	93.00±8.14	101.14	51.20	2.0	25.469	8.2
19	102.20±8.57	110.77	90.78	1.3	22.941	8.2
20	23.60±1.32	24.92	1.50	16.6	2.623	7.5
21	70.80±6.54	77.34	0.99	78.1	6.108	7.8
22	61.10±4.10	65.20	513.00	0.1	-49.258	–
23	92.30±7.18	99.48	43.88	2.3	27.800	8.2
24	80.40±7.41	87.81	1.48	59.3	24.863	8.2

**Table 5.12:** Summarization of earthquake potential variation (when uncertainty in GPS horizontal velocities is considered) at fixed 25 km seismogenic depth; dash (–) in the earthquake potential columns denote no seismic potential.

Area	Earthquake potential using $(\dot{M}_0^g)_{min}$	Earthquake potential using $(\dot{M}_0^g)_{max}$	Earthquake potential range ( $M_w$ )
1	7.6	7.7	7.6–7.7
2	7.7	7.7	7.7
3	7.7	7.8	7.7–7.8
4	7.4	7.5	7.4–7.5
5	7.5	7.5	7.5
6	–	6.9	6.9
7	–	6.8	6.8
8	7.8	7.8	7.8
9	7.5	7.6	7.5–7.6
10	–	7.0	7.0
11	7.7	7.8	7.7–7.8
12	–	–	–
13	8.1	8.1	8.1
14	8.0	8.0	8.0
15	7.0	7.5	7.0–7.5
16	6.5	6.7	6.5–6.7
17	7.2	7.3	7.2–7.3
18	8.1	8.2	8.1–8.2
19	7.8	8.2	7.8–8.2
20	7.5	7.5	7.5
21	7.7	7.8	7.7–7.8

22	–	–	–
23	8.1	8.2	8.1–8.2
24	8.1	8.2	8.1–8.2

**Table 5.13:** Geodetic and seismic moment rates, and moment rate ratio using the seismic and aseismic contribution in the total strain accumulation (at a fixed depth 25 km).

Area	$(\dot{M}_0^g)_{Seismic}$ ( $10^{17}$ Nm/yr)	$(\dot{M}_0^g)_{Aseismic}$ ( $10^{17}$ Nm/yr)	$\dot{M}_0^s$ ( $10^{17}$ Nm/yr)	$\frac{(\dot{M}_0^g)_{Seismic}}{\dot{M}_0^s}$	$\frac{(\dot{M}_0^g)_{Aseismic}}{\dot{M}_0^s}$
1	58.91±5.60	39.27±3.73	19.12	3.1	2.05
2	46.50±2.06	31.00±1.37	6.57	7.1	4.72
3	83.50±7.81	55.67±5.21	3.84	21.7	14.50
4	38.20±2.09	25.47±1.39	0.59	65.1	43.16
5	25.30±2.24	16.87±1.49	0.37	68.6	45.59
6	28.50±2.37	19.00±1.58	27.35	1.1	0.69
7	80.50±4.46	53.67±2.97	75.20	1.1	0.71
8	66.40±3.14	44.27±2.09	1.14	58.4	38.83
9	26.90±1.25	17.93±0.83	10.30	2.6	1.74
10	54.90±2.89	36.60±1.93	50.90	1.1	0.72
11	32.90±1.16	21.93±0.77	0.62	53.1	35.38
12	51.80±3.52	34.53±2.35	88.39	0.6	0.39
13	63.50±2.19	42.33±1.46	8.70	7.3	4.87
14	76.90±3.12	51.27±2.08	6.10	12.6	8.40
15	22.60±1.17	15.07±0.78	20.67	1.1	0.73
16	23.90±1.76	15.93±1.17	18.8	1.3	0.85
17	16.70±1.39	11.13±0.93	2.82	5.9	3.95
18	93.00±8.14	62.00±5.43	51.20	1.8	1.21

19	102.20±8.57	68.13±5.71	90.78	1.1	0.75
20	23.60±1.32	15.73±0.88	1.50	15.7	10.49
21	70.80±6.54	47.20±4.36	0.99	71.5	47.68
22	61.10±4.10	40.73±2.73	513.00	0.1	0.08
23	92.30±7.18	61.53±4.79	43.88	2.1	1.40
24	80.40±7.41	53.60±4.94	1.48	54.3	36.22

**Table 5.14:** Geodetic and seismic moments and earthquake potential using the seismogenic depth as 25 km ( $\geq 900$  years); dash (–) in the earthquake potential columns denote no seismic potential.

Area	$(\dot{M}_0)_{Seismic}$ ( $10^{20}$ Nm)	$(\dot{M}_0)_{Aseismic}$ ( $10^{20}$ Nm)	Earthquake Potential ( $M_w$ ) <sub>Seismic</sub>	Earthquake Potential ( $M_w$ ) <sub>Aseismic</sub>
1	4.258	2.156	7.6	7.5
2	4.911	3.005	7.7	7.6
3	5.576	5.960	7.7	7.8
4	1.993	1.468	7.4	7.4
5	2.244	1.452	7.5	7.4
6	0.081	–3.791	6.5	–
7	0.005	–10.056	5.7	–
8	5.873	15.008	7.7	8.1
9	2.490	1.145	7.5	7.3
10	0.100	–2.731	6.5	–
11	5.165	12.639	7.7	8.0
12	–7.867	–11.579	–	–
13	16.166	9.922	8.0	7.9
14	14.160	4.607	8.0	7.7

15	1.177	-0.577	7.3	–
16	0.107	-0.097	6.6	–
17	0.902	0.657	7.2	7.1
18	21.318	5.508	8.1	7.8
19	15.074	-20.790	8.0	–
20	2.475	1.594	7.5	7.4
21	5.585	3.928	7.7	7.7
22	-49.709	-87.842	–	–
23	24.210	3.089	8.2	7.6
24	22.729	18.346	8.2	8.1

From the derived earthquake potential values in the above tables (Table 5.2 to Table 5.14), the following points are noted.

- **Varying the seismogenic depth (Table 5.2 to Table 5.5)**

When the earthquake depth is varied from 20 km to 35 km, it is observed that the earthquake potential is generally consistent (i.e.,  $\pm 0.1$ ), except for a few regions such as Sec-6, Sec-7, Sec-10, and Sec-19 (Table 5.5). In these regions, the seismic moment rates are observed to be higher than the corresponding geodetic moment rates when the seismogenic depth is chosen as 20 km. Additionally, in Sec-15, there is a notable variation in the earthquake potential ( $M_w=6.8$  to  $M_w=7.8$ ), probably due to the lesser number of seismic events in this section.

- **Varying the length of catalog (Table 5.6 to Table 5.9)**

First, it is assumed that the considered catalog spanning 900 years of seismicity data is long enough to correspond one seismic cycle of great earthquakes based on the available literature [e.g., 31, 40, 161, 219, 227, 277].

Further, to account for the uncertainty due to different catalog length, the earthquake potential is calculated based on three different catalog lengths, such as  $\leq 200$  years,  $\sim 500$  years, and  $\geq 900$  years. The earthquake potential does change while choosing 500 years and 900 years of catalog span, though a minor difference in

potential is noted in the Sec-18. However, seismic potential shows significant variation with  $\leq 200$  years of catalog in Sec-6 ( $M_w=7.6$ ) and Sec-7 ( $M_w=7.8$ ), and more importantly in Sec-12, where it shows potential of a strong ( $M_w=7.8$ ) earthquake. Apart from this, the earthquake potential in all other segments (e.g., Sec-1 to Sec-5, Sec-9 to Sec-11, Sec-13 to Sec-17, and Sec-19 to Sec-23) remains same for all catalog spans ( $\leq 200$  years,  $\sim 500$  years, and  $\geq 900$  years).

- **Considering the upper and lower limits of geodetic moment rate (Table 5.10 to Table 5.12)**

When the range of the geodetic moment rate for a specific segment is considered, it is observed that the current earthquake potential in all segments remains consistent except for Sec-6, Sec-7, and Sec-10, where the seismic moment rates are observed to be higher than the corresponding geodetic moment rates (Table 5.12).

- **Considering the aseismic contribution in the total strain accumulation (Table 5.13 to Table 5.14)**

When the aseismic contribution in the total strain (i.e., 1/3 of total strain rate is released aseismically) is considered, it is observed that the geodetic moment rate and consequent moment ratio have reduced consistently in all segments. However, the earthquake potential does not change significantly, except Sec-6, Sec-7, Sec-10, Sec-15, Sec-16, and Sec-19, where the lack of earthquake potential indicates that almost all the stored energy has been released through the  $\sim 900$  years of seismicity.

## 5.6 Summary

This chapter has concentrated on two key parameters, geodetic measurements, and historical seismicity, for the contemporary seismic hazard assessment along the Himalayan arc. While there is no simple translation of crustal strain rates into the seismic hazard, the moment rate as derived from seismic or geodetic observations has an impactful bearing on the earthquake hazard evaluation [167, 303].

The moment deficit rate in the present analysis varies from  $1.15 \times 10^{17}$  Nm/yr to  $7.97 \times 10^{18}$  Nm/yr which corresponds to earthquakes of magnitude 5.7–8.2 along the northwest to northeast Himalaya (Table 5.1). Moreover, the estimated earthquake potential is largely consistent to the changes of the seismogenic thickness as well as to the geodetic moment rate variation due to the uncertainty in GPS horizontal signals, except

for a few segments. The moment rate ratio derived from geodetic to seismic moment rates in zones Sec-4, Sec-5, Sec-8, Sec-11, Sec-21, and Sec-24 is comparatively high, possibly due to some non-reported events or inherent complex tectonic processes, such as the aseismic deformation, influence of subducting ridges, and so on [84, 86, 213, 275]. In the current study, the contribution from aseismic deformation in the total strain accumulation is not considered due to the lack of proper evidence, though the possible impact of aseismic activity on earthquake potential is discussed in terms of the sensitivity analysis. Non-inclusion of aseismic deformation in total strain is in contrast to Stevens and Avouac (2016) [276] who have assumed that one-third of the moment buildup rate is released aseismically. The consideration of non-inclusion of aseismic activity is partially supported by various previous studies, such as Bilham et al. (1997) [35], Bird and Kagan (2004) [36], Schiffman et al. (2013) [254], Lindsey et al. (2018) [154], Sreejith et al. (2018) [272], and Li et al. (2019) [152], who have reported that there is no prominent evidence of aseismic activity in their respective study regions.

Bilham (2019) [30] has suggested a possible magnitude range of 7.8–8.5 along 15 seismogenic zones of the Himalayan arc, while in the current study, a possible magnitude range of 5.7–8.2 is observed along 24 seismogenic zones. Nevertheless, in both studies, the Kashmir and Kathmandu regions are deemed to have low potential, whereas the central Himalayan zones appear to have high seismic potential. On the other side, the present segmentation-based approach is very similar to the method used by Bungum et al. (2017) [43], except the number of seismogenic segments. They divided the entire arc into six segments, whereas the present analysis has considered 24 segments in order to account for the regional effect of energy release in recent large events. In almost all segments, there is a clear discrepancy in geodetic moment rate as well as moment rate ratio estimation. This could be due to the higher resolution of geodetic data or smaller segment size in the present analysis. Specifically, the disparity is clearly evident in all those segments which encompass the rupture areas of recent large sized earthquakes (e.g., Sec-7 in Kashmir, Sec-10 in eastern Himachal, Sec-12 in Garhwal, and Sec-22 in eastern Nepal) (Fig. 5.5). In eastern Nepal, unlike the estimation of Bungum et al. (2017) [43], it is observed that the accumulated energy is mostly released in the 1934 Nepal-Bihar and the 2015 Gorkha events.

As a summary, the present study determines earthquake potential variation along different segments of the Himalayan arc. The segments with high seismic potential are

observed to correspond the postulated seismic gaps. Alike the continental collision appears to be segmented [84, 93], the earthquake potential appears to be distributed over different segments [93, 138, 182]. The results presented here provide invaluable inputs to the time-dependent seismic hazard analysis in terms of the influence of previous large ruptures and spatial distribution of current earthquake potential.

The present chapter has discussed the spatial distribution of earthquake potential along the Himalayan arc by comparing geodetic and seismic moment rates. It may be noted that in Chapter 3 to Chapter 5, the crustal deformation analysis and earthquake potential analysis are based on the geodetic technique. However, the next chapter, Chapter 6, will present a statistical perspective of contemporary earthquake potential along the Himalayan arc.